

# Model Based Residual Policy Learning with Applications to Antenna Control

**Viktor Eriksson Möllerstedt**

*was with KTH Royal Institute of Technology*

VIKTOR.MOLLERSTEDT@HOTMAIL.COM

**Alessio Russo**

*Division of Decision and Control Systems, KTH Royal Institute of Technology*

ALESSIOR@KTH.SE

**Maxime Bouton**

*Ericsson Research*

MAXIME.BOUTON@ERICSSON.COM

**Editors:** R. Firooz, N. Mehr, E. Yel, R. Antonova, J. Bohg, M. Schwager, M. Kochenderfer

## Abstract

Non-differentiable controllers and rule-based policies are widely used for controlling real systems such as robots and telecommunication networks. In this paper, we present a practical reinforcement learning method which improves upon such existing policies with a model-based approach for better sample efficiency. Our method significantly outperforms state-of-the-art model-based methods, in terms of sample efficiency, on several widely used robotic benchmark tasks. We also demonstrate the effectiveness of our approach on a control problem in the telecommunications domain, where model-based methods have not previously been explored. Experimental results indicate that a strong initial performance can be achieved and combined with improved sample efficiency. We further motivate the design of our algorithm with a theoretical lower bound on the performance.

**Keywords:** model-based reinforcement learning; sample efficiency; mobile networks; robotics;

## 1. Introduction

Reinforcement learning (RL) is a powerful and flexible method for automatically learning to solve control tasks. However, training an RL agent requires a lot of data, which usually involves sampling from an environment. In addition, agents initially tend to have poor performance for multiple iterations before learning useful behaviors. In real world applications, sampling data from an environment can be costly, time-consuming, and excessively risky. Instead, other approaches relying on hand-engineered policies or control theoretic methods can be used at the expense of scalability and performance (Dulac-Arnold et al., 2021). Addressing sample efficiency, and the poor initial performance of the RL agents, is necessary in order to use this technology in physical systems.

There exist several approaches to address sample efficiency in RL. A practical approach is to use a model of the environment to generate training data for the agent, thus lowering the need for sampling data points from the real environment. Model-based approaches, such as MBPO (Janner et al., 2019a), and Dreamer (Hafner et al., 2020), learn such a model using real environment data and use it to generate extra training data for a model-free RL algorithm. These methods have shown impressive gains in sample efficiency, but just as many other RL methods, they suffer from poor initial performance because the agent starts by exploring the environment with random actions. Other methods leverage a baseline policy during training (Silver et al., 2018; Hester et al., 2018), which can lead to strong initial performances and in some cases an increase in sample efficiency. *Residual*

*Policy Learning* (RPL) (Silver et al., 2018) consists of learning a correction term to a deterministic baseline policy, which does not need to be differentiable.

With the goal of further increasing the sample efficiency while maintaining a strong initial performance, we expand upon ideas from both model-based methods and methods that use a baseline policy. We propose a practical model-based RL algorithm, and show how it can be applied to a real world problem of controlling base station antennas in a telecommunication network. Interestingly, recent work in this domain has shown that RL agents can outperform traditional rule-based policies. One such example is the coverage and capacity optimization problem, where the agent controls the down-tilt of antennas in order to optimize the KPIs coverage, capacity and quality (Vannella et al., 2021; Buenestado et al., 2017). The existence of rule-based strategies for this problem is a strong asset that can be used in combination with RL algorithms.

Previous works have addressed the problem of antenna tilt control with RL by using standard algorithms, such as DQN Mnih et al. (2013), or focused on the multi-agent aspect (Farooq et al., 2019; Bouton et al., 2021; Dandanov et al., 2017) without considering sample efficiency. Another body of literature has investigated safe reinforcement learning approaches (Nikou et al., 2021; Aumayr et al., 2021). For instance, Vannella et al. used a rule-based policy as a behavioral policy to gather data from the environment. This data was then used to learn a greedy using off-policy methods. Even though these methods make the training process safer, they do not necessarily increase the sample efficiency. For the antenna control problem, sample efficiency is of core importance to enable learning in the real world, but also of practical importance when learning in simulation, since network simulation usually involves expensive computation. The algorithm proposed in this paper specifically targets this aspect, along with the initial performance of the agent, and can be combined with previous works that considers safety and multi-agent coordination.

In this work, we present a novel method which uses a model-based approach to learn a correction term to a baseline policy. We show how the RPL idea can be extended to stochastic policies, and that we get cumulative gain by combining it with model-based methods. A theoretical analysis of the algorithm performance bound is provided. We then evaluate our approach on a problem of controlling antennas in a telecommunication network, which we model as a continuous action problem. We empirically show that our proposed algorithm outperforms the state-of-the-art on this problem in terms of sample efficiency, which makes it a better alternative for real world deployment. Finally, we evaluate the method on several robotic control tasks in the MuJoCo environment, frequently outperforming state-of-the art model-based methods in terms of sample efficiency. For each experiment, ablation studies show the contributions of both the residual learning and the model based components.

## 2. Background

**Markov Decision Processes.** We model the problem as a Markov Decision Process (MDP):  $(\mathcal{S}, \mathcal{A}, r, p, \rho_0)$ . Here,  $\mathcal{S}$  is the state-space,  $\mathcal{A}$  the action-space,  $r : \mathcal{S} \times \mathcal{A} \times \mathcal{S} \rightarrow \mathbb{R}$  the reward function,  $p : \mathcal{S} \times \mathcal{A} \rightarrow \Delta(\mathcal{S})$  the transition probability function (also known as transition dynamics;  $\Delta(\mathcal{S})$  is the space of probability distributions with support  $\mathcal{S}$ ), and  $\rho_0(s)$  is the initial state probability distribution. At step  $t$ , the agent observes the current state  $s_t$  of the system, and selects  $a_t$  according to a stationary Markov policy  $\pi : \mathcal{S} \rightarrow \Delta(\mathcal{A})$ . The goal of the agent is to find a policy  $\pi$  that maximizes the total discounted reward collected from the environment. For a discount factor  $\gamma \in (0, 1)$ , we define the discounted value of  $\pi$  as  $V^\pi(\rho_0) = \mathbb{E}_{s_0 \sim \rho_0} \left[ \sum_{t=0}^{\infty} \gamma^t r(s_t, a_t, s_{t+1}) \mid s_{t+1} \sim p(\cdot | s_t, a_t), a_t \sim \pi(\cdot | s_t) \right]$ .

**Residual policy learning (RPL).** RPL consists in learning a deterministic correction term  $\pi_c$  to a baseline policy  $\pi_b$  (Silver et al., 2018). The baseline policy  $\pi_b$  does not need to be differentiable. This baseline policy can represent prior knowledge in the form of an existing controller. The baseline may come from a hand-engineered method, a control theoretic approach or result from a reinforcement learning agent trained under different conditions.

**Model-based RL.** In RL problems the transition function is usually unknown, and in model-based RL it is explicitly learned during training by learning a parameter  $\theta$  of a model  $p_\theta$  such that  $p_\theta \approx p$ . Specifically, for a given buffer of experiences  $(s_t, a_t, r_t, s_{t+1}) \in \mathcal{B}$ , a model  $p_\theta$  is usually learned by maximizing the log-likelihood of the data so that  $\theta \leftarrow \arg \max_\theta \mathbb{E}_{(s, a, r, s') \sim \mathcal{B}} [\log \mathcal{L}(s, a, r, s'; \theta)]$ , where  $\mathcal{L}$  is the likelihood function. Using this learned model, it is possible to use model-free methods to learn a policy  $\pi$  using data sampled from  $p_\theta$  (for more details, see also Janner et al. 2019a). The benefit of this approach is that the user can significantly reduce the number of experiences sampled from the true environment, which may be challenging or costly to acquire in certain scenarios. Finally, note that the reward function is often assumed to be known, and other times it must be learned along with the transition dynamics. In this work, we consider both cases.

### 3. Method

In this work <sup>1</sup>, we improve on the residual-policy learning concept by considering a model-based approach. The goal is to minimize the number of interactions with the true environment by using (1) prior knowledge in the form of a baseline policy, and (2) a model-based approach to train the policy. Our method consists of training a correction term to a baseline policy using model-based RL. By using a baseline policy, the aim is to achieve a strong initial performance and to guide the training in a sound direction. The model-based component is added to reduce the number of samples needed from the true environment to train the correction term. In the following sections, we first explain how the policies are combined, and later explain the training process of the method.

#### 3.1. Stochastic Residual Policy Learning

As explained in Section 2, Residual Policy Learning combines a baseline policy  $\pi_b$  with a correction term  $\pi_c$ . The baseline policy does not need to be differentiable, and can be of any form. In Silver et al. the authors consider deterministic policies, whereas we focus on stochastic policies (such as PPO (Schulman et al., 2017) or SAC (Haarnoja et al., 2018a)) that make use of an actor-critic training procedure. In fact, these algorithms have empirically shown to lead to more stable training than deterministic policies trained, for example, using DDPG. Combining a stochastic policy  $\pi_c$  with a baseline policy  $\pi_b$ , which does not necessarily need to be stochastic, can be done in different ways depending on the problem of interest. In this work, we focus on problems with continuous action spaces, and therefore at step  $t$  the action chosen by the agent can be represented as  $a_t = f(a_t^c, a_t^b)$ , where  $(a_t^c, a_t^b)$  are, respectively, the actions chosen by the correction term and the baseline term at time  $t$ . The function  $f$  combines the two actions and can be customized.

For example, assuming that the correction term is represented by a Gaussian distribution of parameters  $\phi = (\mu, \sigma)$ , and the baseline term is deterministic, if  $f(x, y) = x + y$  the overall policy at time  $t$  can be expressed as  $\pi_\phi^b(\cdot | s_t) = \mathcal{N}(\mu(s_t) + a_t^b, \sigma^2(s_t))$ , where the parameters  $(\mu, \sigma)$  are

---

1. The appendix can be found here <https://arxiv.org/abs/2211.08796> (it contains all the proofs and numerical details).

**Algorithm 1** Model-Based Residual Policy Learning (MBRPL)**Input:** Baseline policy  $\pi_b$ , parameters of the correction term  $\phi = (\mu, \sigma)$ 

- 1: Initialize transition model  $p_\theta$ , and initialize critic  $Q_\psi$  parametrized by  $\psi$ .
- 2: Initialize replay buffer  $\mathcal{B}$
- 3: **for** epoch = 1, ...,  $N$  **do**
- 4:   Sample experiences from the true environment using  $\pi_\phi^b$  and add them to  $\mathcal{B}$
- 5:   Train  $p_\theta$  on  $\mathcal{B}$  using maximum-likelihood
- 6:   Use  $(p_\theta, r, \pi_\phi^b)$  to generate trajectories and train  $(\pi_\phi^b, Q_\psi)$  using off-policy actor critic methods
- 7: **end for**

learned online using classical policy learning methods, such as SAC. If the baseline policy also represents a Gaussian distribution with parameters  $\mathcal{N}(\mu_b, \sigma_b^2)$ , independent of the correction term, then we simply derive  $\pi_\phi^b(\cdot|s) = \mathcal{N}(\mu_b(s) + \mu(s), \sigma_b^2(s) + \sigma^2(s))$ . The policy is initialized to closely follow the baseline  $\pi_b$ . For instance, if the residual is a neural network that outputs the parameters of a Gaussian distribution, the initialization sets the weights of the final linear layer close to 0. This leads to a stronger initial performance, but the critic is randomly initialized. This random initialization of the critic can lead to an initial performance drop, since the critic guides the training of the actor in the "wrong" direction. To overcome this problem, just like in RPL, we let the critic train while keeping the policy unchanged during the initial phase. The number of training steps during which the critic trains with a constant policy is denoted Critic Burn-In (CBI). In summary, this approach extends the existing RPL algorithm to support training stochastic policies and use more recent model-free RL algorithms such as SAC to learn the policy residual.

### 3.2. Model-Based Residual Policy Learning (MBRPL)

Motivated by maximizing sample efficiency, we propose to combine stochastic RPL with a model-based approach. We give a high level description of the algorithm in Algorithm 1. The training method consists of alternating between learning the dynamics, predicting future states and rewards, and training the residual policy and critic on the real and predicted data. Finally, we provide a theoretical performance bound on the performance of the policy, providing new insights on the stochastic residual policy approach.

A function approximator  $p_\theta$  is introduced to model the true environment, which is trained by maximizing the log-likelihood between generated data and true data sampled from the environment. The training of the model is done at regular interval throughout the training. The frequency at which the model is trained and the number of data points used to train it at each step are hyperparameters of the algorithm and are different depending on the environment (see the experiment section for details). This part of the method is similar to existing model-based RL methods (Janner et al., 2019a).

The policy is formed using stochastic residual policy learning, and the correction term is trained using trajectories generated by the learned model  $p_\theta$  using off-policy model free methods. In particular, we use soft-actor critic to train the stochastic policy residual. All the hyperparameters and design choices (e.g. model representation) will be discussed in the experiment section and appendix.

**Theoretical performance.** We now theoretically analyze the performance bound of the learned policy compared to both how close the baseline policy is to the optimal solution and how close the model is to the true transition model. Since the baseline policy is not necessarily created using the

same environment  $M$  where the corrected policy will operate on, but possibly a different one  $M_b$ , we analyzed the performance of the corrected policy in  $M$  depending on its performance in  $M_b$ .

To derive a performance bound, we first consider the following lemma that bounds the performance of a generic policy  $\pi$  in two similar environments  $M$  and  $M_b$ , with the same reward, and different transition functions  $P_0$  and  $P_1$ . Assuming that  $(P_0, P_1)$  are similar in the Kullback-Leibler sense, we derive the following result (the proof is provided in the appendix).

**Lemma 1** *Consider two MDPs  $M = (r, P_1)$  and  $M_b = (r, P_0)$  and a Markov stationary policy  $\pi$ . Let  $r \in [0, 1]$ , and assume that  $KL(P_0(s, a), P_1(s, a)) = \mathbb{E}_{s' \sim P_0(\cdot|s, a)} \left[ \log \frac{P_0(s'|s, a)}{P_1(s'|s, a)} \right] \leq \varepsilon$  for all  $(s, a)$ . Then  $|V_{M_b}^\pi(\mu) - V_M^\pi(\mu)| \leq \sqrt{2\varepsilon} \frac{\gamma}{1-\gamma} \|V_{M_b}^\pi\|_\infty$  for any distribution  $\mu$  of the initial state.*

Given this performance bound, the idea is to evaluate the performance of the corrected policy  $\pi_\phi^b$  knowing the performance of the baseline term  $\pi_b$  in the environment  $M_b$  in which it was trained. Similarly as before, assuming that the correction policy and the baseline policy are close in the KL-sense, we derive the following.

**Lemma 2** *Consider two MDPs  $M = (r, P)$  and  $M_b = (r, P_0)$ , with  $r \in [0, 1]$ , that satisfy  $KL(P_0(s, a), P(s, a)) \leq \varepsilon_0$  for all  $(s, a) \in S \times A$ . Let  $\pi_b$  be a Markov policy trained on  $M_b$ , and let its average total discounted reward be  $V_{M_b}^{\pi_b}(\mu)$ , for some initial distribution of the state  $\mu$  and discount factor  $\gamma$ . Assume that  $\max_s KL(\pi_\phi^b(s), \pi_b(s)) \leq \varepsilon_\pi$ . Then*

$$V_{M, \gamma}^{\pi_\phi^b}(\mu) \geq V_{M_b, \gamma}^{\pi_b}(\mu) - \frac{\sqrt{2}}{1-\gamma} \left( \frac{\sqrt{\varepsilon_\pi}}{(1-\gamma)} + \gamma \sqrt{\varepsilon_0} \|V_{M_b, \gamma}^{\pi_b}\|_\infty \right) \quad (1)$$

**Proof** Note that  $|V_{M, \gamma}^{\pi_\phi^b}(\mu) - V_{M_b, \gamma}^{\pi_b}(\mu)| = |V_{M, \gamma}^{\pi_\phi^b}(\mu) - V_{M_b, \gamma}^{\pi_b}(\mu) \pm V_{M_b, \gamma}^{\pi_b}(\mu)| \leq |V_{M, \gamma}^{\pi_\phi^b}(\mu) - V_{M, \gamma}^{\pi_b}(\mu)| + |V_{M_b, \gamma}^{\pi_b}(\mu) - V_{M, \gamma}^{\pi_b}(\mu)|$ . The second term can be bounded using Lemma 1 as  $|V_{M_b, \gamma}^{\pi_b}(\mu) - V_{M, \gamma}^{\pi_b}(\mu)| \leq \sqrt{2\varepsilon_0\gamma} \|V_{M_b, \gamma}^{\pi_b}\|_\infty$ . The first term can be bound as in (Janner et al., 2019b, Lemma B.3), i.e.,  $|V_{M, \gamma}^{\pi_\phi^b}(\mu) - V_{M, \gamma}^{\pi_b}(\mu)| \leq \sqrt{2\varepsilon_\pi} \frac{1}{(1-\gamma)^2}$ , where we also made use of Pinsker's inequality. We conclude that  $|V_{M, \gamma}^{\pi_\phi^b}(\mu) - V_{M_b, \gamma}^{\pi_b}(\mu)| \leq \frac{\sqrt{2\varepsilon_\pi}}{(1-\gamma)^2} + \sqrt{2\varepsilon_0} \frac{\gamma}{1-\gamma} \|V_{M_b, \gamma}^{\pi_b}\|_\infty$ , from which the result follows. ■

Lemma 2 tells us that if the two policies are similar enough, the performance of the corrected policy in  $M$  is comparable to that of the baseline in  $M_b$ , if the two environments are not too different. This result motivates learning a correction term to the baseline policy in an environment in which the baseline performs suboptimally. Initializing the correction term to 0 at the beginning of training encourages similarity of the corrected policy and the baseline. In the next section, we empirically demonstrate the strength of this approach.

## 4. Experiments

In this section, we illustrate the application of our method to a realistic telecommunication network problem, coverage and capacity optimization problem via antenna tilt control. Additionally, we have also evaluated our method on several benchmark robotic control tasks from the MuJoCo library (Todorov et al., 2012). We examined several questions: whether MBRPL was generally more sample efficient than existing methods, whether it could maintain a strong initial performance, and whether both the residual and model based components contribute to a performance improvement. All the experiments were conducted using proprietary code. For further details, please refer to the authors.

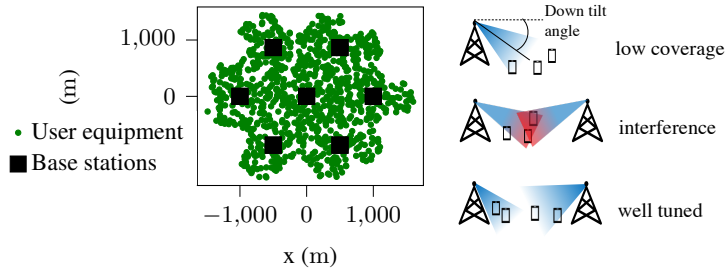


Figure 1: **Left:** aerial view of the networks. 3 antennas are attached to each base station, pointing in different directions. **Right:** effect of changing the tilt angle on coverage and quality.

#### 4.1. Antenna Tilt Control

In this section, we study the sample efficiency of MBRPL on a coverage and capacity optimization task via control of antenna tilt. We make a comparison against several well-known model-free baselines, and perform an ablation study. In addition, we study how the critic burn-in affects the initial performance of MBRPL.

##### 4.1.1. PROBLEM FORMULATION

**The antenna environment.** Mobile telecommunication networks are composed of a number of *base stations* to which one or several antennas are mounted. The antennas transfer data to and from several users, such as cellphones and computers. A user decides which antenna to attach to based on signal strength. Users attached to the same antenna form a *cell*. In the coverage and capacity optimization problem, the goal is to control the tilt of the antenna such that all users have good coverage, good signal quality, and that many users can send and receive data at the same time. When adjusting the parameters of the antennas, these three quantities will be affected, and the down-tilt angle  $w$  is the one of the most influential parameters (Buenestado et al., 2017; Vannella et al., 2021; Dreifuerst et al., 2021). Fig. 1 (right) illustrates its influence on coverage and signal quality.

The antenna tilt problem can be modeled as an MDP, and it is inherently a multi-agent problem, since there are many antennas interacting in the same environment. We approached the problem of controlling multiple antennas via parameter sharing. Each antenna represents an agent, but a single policy and model was trained on the data gathered from all antennas. Other lines of work address the problem of coordinating antennas (Bouton et al., 2021), and combining those approaches with our algorithm is left for future work. We used the following MDP formulation:

**Observation space.** The agent observes its current tilt angle  $w$ , and three key performance indicators (KPIs): coverage, capacity and quality for the users it is serving. Coverage is measured as an average of the logarithm of the reference signal received power (RSRP) for all served users; capacity as an average of the logarithm throughput; quality through the average of the logarithm signal to interference and noise ratio (Dreifuerst et al., 2021; Farooq et al., 2019; Bouton et al., 2021). We apply this log-transform to better condition the numerical values. The dimensionality of the observation space is 4. More details of the mathematical models used to calculate the signal strength and quality are provided in the appendix.

**Action space.** The agent outputs one continuous change of tilt-angle  $(\Delta w)_i \in [-1^\circ, 1^\circ]$  for each antenna  $i$ . The tilt-angle  $w_i$  for the  $i$ -th antenna is limited to lie between  $0^\circ$  and  $15^\circ$ .

**Reward function.** The reward function at time  $t$  is a sum of the coverage, capacity and quality at time  $t + 1$ . Each KPI was approximately normalized to have mean 0 and standard deviation 1. The mean and standard deviation were measured empirically.

The antenna environment was simulated using a proprietary system level LTE network simulator relying on a map-based propagation model to compute the signal received by each user (Asplund et al., 2018). The network was built as a hexagonal grid of 7 base stations with 3 antennas each (21 agents). 1000 static users were uniformly distributed across the environment, see Fig. 1 (left). The environment is a 50-50 split of indoor and outdoor environment, with buildings placed uniformly at random across the map. Buildings affects how the signal propagates between the antenna and a user (check the appendix for details). The buildings were excluded from the figure to prevent cluttering.

#### 4.1.2. EXPERIMENTAL SETUP

We compared the sample efficiency and performance at convergence of MBRPL against several baselines. SAC is a model-free state-of-the-art RL algorithm (Haarnoja et al., 2018a,b). DQN (Mnih et al., 2013) is a well-known discrete action-space model-free method used in several previous works on RL for antenna down-tilt control (Vannella et al., 2021; Bouton et al., 2021; Aumayr et al., 2021). For DQN, the action space is changed to update the tilt by increments of  $\{-1^\circ, 0^\circ, 1^\circ\}$ . We also compare to ablations of our method: model-based SAC (MBSAC) and stochastic RPL (SRPL). MBSAC uses only the model-based part of the algorithm to train a SAC agent. SRPL learns a residual policy to a stochastic baseline policy using SAC. Finally, we study the effect of the critic burn-in parameter on MBRPL. This parameter controls how many steps the policy is frozen at the baseline policy while the critic trains.

**Baseline policy.** As a baseline policy for MBRPL and SRPL, we use the policy of a SAC agent trained on a modified version of the environment, where all buildings were removed. The resulting policy was better than a random policy, but with suboptimal performance in the true environment. The baseline has the same observation and action space as our agent.

**Model-based approach.** The transition model used by MBRPL and MBSAC is a single neural network which outputs the mean and variances of a Gaussian distribution, trained with the MSE loss between the true and predicted next state. Alternatively, one could have tried using an ensemble of models as in MBPO, but we found out that a single model was enough for learning a performant policy in the antenna environment. The details of the hyperparameters can be found in the appendix. For the MBSAC baseline, we used the same model training hyperparameters.

**Training.** We let each method train for 10 000 steps across 5 random seeds. The positions of the users and buildings were uniformly randomly generated at the start of each experiment, and the tilt of the antennas were initialized uniformly at random within the allowed range. For one step of the environment, we collect a transition sample from all 21 antennas and add them to the replay buffer. We began by tuning the hyperparameters of the benchmark algorithms (SAC, DDPG, DQN), and then used the same parameters for MBRPL and the ablations. Our methods require some additional settings, such as choice of baseline policy, critic burn-in and prediction horizon. The baseline policy was designed such that it is better than random, but still suboptimal. Details of the hyperparameters can be found in the appendix.

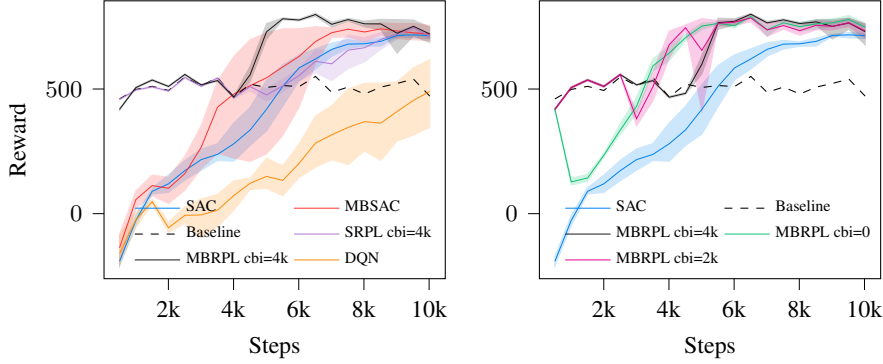


Figure 2: **Left:** MBRPL compared to the benchmarks SAC, DQN, and the ablations MBSAC and SRPL. **Right:** effect of the critic burn-in period on MBRPL. The lines are the mean values, and the shaded areas the 95 % confidence intervals across 5 seeds. The reward is a running average over the last 100 episodes.

#### 4.1.3. RESULTS

A comparison of MBRPL to the benchmarks and the ablations can be seen in Fig. 2 (left). MBRPL is the most sample efficient by far, converging at around 5500 steps. SAC, MBSAC and SRPL converge at around 9000 steps. DQN did not converge until the step limit was reached. DDPG was unable to learn at all, and has been excluded from the plot. The baseline policy reached an average reward of  $682 \pm 57$  (1 std) in the environment without buildings, on which it was trained. In the evaluation environment of Fig. 2 it collected an average reward of  $508 \pm 26$  (1 std).

MBSAC is not significantly more sample efficient on average than SAC, in spite of using 10 times as much data to learn. There is a large variance in performance across the different seeds. Since SAC is not having similar issues, it is reasonable to assume that the model-based component is causing it, and may be due to poor model accuracy. Epistemic uncertainty in model prediction could be addressed by using an ensemble of transition models, as in MBPO. Both MBRPL and SRPL have a much stronger initial performance due to the baseline policy, but SRPL is not more sample efficient than SAC. This highlights the strength of the combined approach of MBRPL. The strong initial policy allows more efficient use of the learned model, increasing sample efficiency significantly.

Figure 2 (right) shows the effect of changing the critic burn-in setting. A low value leads to a large initial dip in performance, most likely caused by the mismatch between actor and critic performance, similar to what was observed in the original RPL paper (Silver et al., 2018). MBRPL is able to recover quickly, and still converges well before SAC. Increasing the critic burn-in reduces the dip, but can delay convergence because the policy training is postponed.

#### 4.2. Robotic control

We examine the sample efficiency and performance at convergence of MBRPL on several control tasks simulated with the MuJoCo physics engine. The problems we study are Hopper, Walker (Tassa et al. (2018)), and Ant with truncated observations.

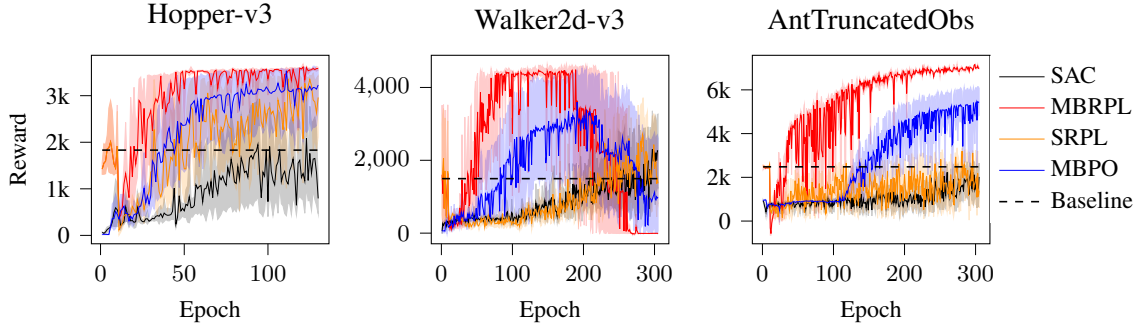


Figure 3: Comparison of MBRPL against the benchmark SAC, and the ablation RSAC on three MuJoCo tasks. MBRPL plays both the role of benchmark and ablation.

#### 4.2.1. EXPERIMENTAL SETUP

We compare against MBPO, SAC and SRPL. MBPO and SAC represent the state-of-the-art within model-based and model-free methods, respectively. SRPL is an ablation of our method (see the section on the antenna tilt problem for more information).

**Baseline policy.** The baseline policy is a SAC agent trained on a version of the environment with lower gravity. It is used by MBRPL and SRPL. We combined the residual policy with the mean of the baseline policy.

**Model-based approach.** Initially, we used a simplified model-based approach to train the residual policy (see the antenna experiment section for more details). We found that the model was unable to learn an accurate enough representation of the environment, resulting in a collapse of the training process. Hence, we decided to use MBPO to train the residual correction term in MBRPL. The transition model in MBPO uses an ensemble of neural networks, which reduces epistemic uncertainty caused by the random initialization of the model weights. In addition, it is trained on all the so-far collected environment data until the validation loss increases each  $k$ :th step. On the antenna tilt environment, we only trained on one batch of data each time step, leading to far fewer model updates. The complexity of the MuJoCo tasks requires putting more effort on the model learning. Using an ensemble trained on all the current environment data yielded models of higher quality.

**Training.** We trained the model-based methods for 130 epochs on Hopper, and 300 epochs on Walker and Truncated Ant. SAC was trained for 1000 and 3000 epochs, respectively. Each epoch consisted of 1000 environment steps. Each experiment was repeated 5 times. We used the MBPO and SAC implementations from MBRL-Lib (Pineda et al., 2021). On Hopper, we used the official MBPO parameters. On Truncated Ant, we had to use the parameters from the MBRL-Lib repository to achieve a similar performance as in the MBPO paper. In the Walker environment, the MBRL-lib parameters gave the better result, but led to a significantly lower maximum reward (25% lower) than the official MBPO implementation, and a decline after around 200 epochs. Our method, MBRPL, used the same parameters as those used for MBPO. It also requires some additional hyperparameters, such as choice of baseline policy and critic burn-in. The parameters can be found in the appendix.

#### 4.2.2. RESULTS

A comparison of MBRPL to the baselines can be seen in Fig. 3. MBRPL was the most sample efficient method on most tasks. The difference in efficiency is especially striking in the Truncated Ant environment, where MBRPL reached a reward of 7000 in 300 epochs, compared to the 5400 of MBPO. MBRPL again outperforms MBPO in the Hopper environment, but the difference in reward when MBRPL converges is smaller. It appears as if it converges to a  $\approx 10\%$  higher reward, and does so in a third of the epochs. In the Walker environment, MBRPL initially vastly outperforms MBPO in terms of sample efficiency. However, the two model-based methods show a decline in performance after around 200 epochs. A possible explanation is a catastrophic forgetting of the policy, or the loss being unstable, as was observed in the Humanoid environment in the MBRL-lib paper.

Another important thing to note is the dip in performance of MBRPL and SRPL during the early stages of the training. It is possible that a larger critic burn-in could have prevented this dip in performance, as was found for the antenna tilt problem. The performance of the baselines in the training and true environment can be seen in Table 1.

Since the only difference between MBPO and this version of MBRPL is the use of the baseline policy, this must be the cause of the increased sample efficiency. By guiding the policy into higher reward regions earlier, it is able to accelerate learning. Interestingly, the model-based component of MBRPL also plays a crucial role - the model-free ablation RSAC is noticeably slower to converge than MBPO. The difference is the most significant on Truncated Ant.

Task	Hopper-v3	Walker2d-v3	AntTruncatedObs
Trained with $g$ :	$7 \text{ m s}^{-2}$	$6 \text{ m s}^{-2}$	$4 \text{ m s}^{-2}$
Reward in training env	$3505 \pm 30$	$3150 \pm 1546$	$4793 \pm 1431$
Reward with $9.81 \text{ m s}^{-2}$	$1831 \pm 780$	$1496 \pm 1533$	$2481 \pm 70$

Table 1: The mean and 1 standard deviation of the reward collected by the baseline policies used for each task in the MuJoCo environment.

## 5. Conclusion

In this work, we have presented a model-based RL method which learns a residual correction term to a baseline policy. Our method outperformed a state-of-the-art model-based method in terms of sample efficiency on most investigated robotic control benchmarks. It also proved effective for optimizing coverage and capacity on an antenna tuning problem. Model-based RL had not previously been tested on that environment, and our method outperformed all benchmarks. Ablation studies show that combining the usage of a baseline policy with a model-based approach leads to higher sample efficiency. A hyperparameter study indicates that the higher initial performance of the baseline policy can be maintained by setting the appropriate critic burn-in, however, further testing is needed to confirm this result. Our results hint that relying on an existing suboptimal controller, paired with a model-based approach, is a viable approach for deploying intelligent control algorithms in real-world applications. Future research directions could involve model residual learning when approximate models are available, as well as extending RPL to discrete action spaces.

## References

Henrik Asplund, Martin Johansson, Magnus Lundevall, and Niklas Jaldén. A set of propagation models for site-specific predictions. In *European Conference on Antennas and Propagation (EuCAP)*, pages 1–5, 2018. doi: 10.1049/cp.2018.0385.

Erik Aumayr, Saman Feghhi, Filippo Vannella, Ezeddin Al Hakim, and Grigoris Iakovidis. A safe reinforcement learning architecture for antenna tilt optimisation. In *2021 IEEE 32nd Annual International Symposium on Personal, Indoor and Mobile Radio Communications (PIMRC)*, pages 1148–1153, 2021. doi: 10.1109/PIMRC50174.2021.9569387.

Maxime Bouton, Hasan Farooq, Julien Forgeat, Shruti Bothe, Meral Shirazipour, and Per Karlsson. Coordinated reinforcement learning for optimizing mobile networks. *NeurIPS Workshop on cooperative AI*, 2021. URL <https://arxiv.org/abs/2109.15175>.

Víctor Buenestado, Matías Toril, Salvador Luna-Ramírez, José María Ruiz-Avilés, and Adriano Mendo. Self-tuning of remote electrical tilts based on call traces for coverage and capacity optimization in LTE. *IEEE Transactions on Vehicular Technology*, 66(5):4315–4326, 2017. doi: 10.1109/TVT.2016.2605380. URL <https://doi.org/10.1109/TVT.2016.2605380>.

Nikolay Dandanov, Hussein Al-Shatri, Anja Klein, and Vladimir Poulkov. Dynamic self-optimization of the antenna tilt for best trade-off between coverage and capacity in mobile networks. *Wirel. Pers. Commun.*, 92(1):251–278, 2017. doi: 10.1007/s11277-016-3849-9. URL <https://doi.org/10.1007/s11277-016-3849-9>.

Ryan M. Dreifuerst, Samuel Daulton, Yuchen Qian, Paul Varkey, Maximilian Balandat, Sanjay Kasturia, Anoop Tomar, Ali Yazdan, Vish Ponnampalam, and Robert W. Heath Jr. Optimizing coverage and capacity in cellular networks using machine learning. In *IEEE International Conference on Acoustics, Speech and Signal Processing, ICASSP*, pages 8138–8142. IEEE, 2021. doi: 10.1109/ICASSP39728.2021.9414155. URL <https://doi.org/10.1109/ICASSP39728.2021.9414155>.

Gabriel Dulac-Arnold, Nir Levine, Daniel J. Mankowitz, Jerry Li, Cosmin Paduraru, Sven Gowal, and Todd Hester. Challenges of real-world reinforcement learning: definitions, benchmarks and analysis. *Mach. Learn.*, 110(9):2419–2468, 2021. doi: 10.1007/s10994-021-05961-4. URL <https://doi.org/10.1007/s10994-021-05961-4>.

Hasan Farooq, Ali Imran, and Mona Jaber. AI empowered smart user association in LTE relays hetnets. In *IEEE International Conference on Communications ICC Workshops*, pages 1–6. IEEE, 2019. doi: 10.1109/ICCW.2019.8756942. URL <https://doi.org/10.1109/ICCW.2019.8756942>.

Tuomas Haarnoja, Aurick Zhou, Pieter Abbeel, and Sergey Levine. Soft actor-critic: Off-policy maximum entropy deep reinforcement learning with a stochastic actor. In Jennifer G. Dy and Andreas Krause, editors, *International Conference on Machine Learning (ICML)*, volume 80 of *Proceedings of Machine Learning Research*, pages 1856–1865. PMLR, 2018a. URL <http://proceedings.mlr.press/v80/haarnoja18b.html>.

Tuomas Haarnoja, Aurick Zhou, Kristian Hartikainen, G. Tucker, Sehoon Ha, Jie Tan, Vikash Kumar, Henry Zhu, Abhishek Gupta, P. Abbeel, and Sergey Levine. Soft actor-critic algorithms and applications. *ArXiv*, abs/1812.05905, 2018b.

Danijar Hafner, Timothy P. Lillicrap, Jimmy Ba, and Mohammad Norouzi. Dream to control: Learning behaviors by latent imagination. In *8th International Conference on Learning Representations, ICLR 2020, Addis Ababa, Ethiopia, April 26-30, 2020*. OpenReview.net, 2020.

Todd Hester, Matej Vecerík, Olivier Pietquin, Marc Lanctot, Tom Schaul, Bilal Piot, Dan Horgan, John Quan, Andrew Sendonaris, Ian Osband, Gabriel Dulac-Arnold, John P. Agapiou, Joel Z. Leibo, and Audrunas Gruslys. Deep q-learning from demonstrations. In Sheila A. McIlraith and Kilian Q. Weinberger, editors, *AAAI Conference on Artificial Intelligence*, pages 3223–3230. AAAI Press, 2018.

Michael Janner, Justin Fu, Marvin Zhang, and Sergey Levine. When to trust your model: Model-based policy optimization. pages 12498–12509, 2019a. URL <https://proceedings.neurips.cc/paper/2019/hash/5faf461eff3099671ad63c6f3f094f7f-Abstract.html>.

Michael Janner, Justin Fu, Marvin Zhang, and Sergey Levine. When to trust your model: Model-based policy optimization. *Advances in Neural Information Processing Systems*, 32, 2019b.

Volodymyr Mnih, Koray Kavukcuoglu, David Silver, Alex Graves, Ioannis Antonoglou, Daan Wierstra, and Martin Riedmiller. Playing atari with deep reinforcement learning. 2013. URL <http://arxiv.org/abs/1312.5602>. cite arxiv:1312.5602Comment: NIPS Deep Learning Workshop 2013.

Alexandros Nikou, Anusha Mujumdar, Marin Orlić, and Aneta Vulgarakis Feljan. Symbolic reinforcement learning for safe ran control. In *Autonomous Agents and Multiagent Systems*, page 1782–1784. International Foundation for Autonomous Agents and Multiagent Systems, 2021. ISBN 9781450383073.

Luis Pineda, Brandon Amos, Amy Zhang, Nathan O. Lambert, and Roberto Calandra. Mbrl-lib: A modular library for model-based reinforcement learning. *CoRR*, abs/2104.10159, 2021. URL <https://arxiv.org/abs/2104.10159>.

John Schulman, Filip Wolski, Prafulla Dhariwal, Alec Radford, and Oleg Klimov. Proximal policy optimization algorithms. *arXiv preprint arXiv:1707.06347*, 2017.

Tom Silver, Kelsey R. Allen, Josh Tenenbaum, and Leslie Pack Kaelbling. Residual policy learning. *CoRR*, abs/1812.06298, 2018. URL <http://arxiv.org/abs/1812.06298>.

Yuval Tassa, Yotam Doron, Alistair Muldal, Tom Erez, Yazhe Li, Diego de Las Casas, David Budden, Abbas Abdolmaleki, Josh Merel, Andrew Lefrancq, Timothy P. Lillicrap, and Martin A. Riedmiller. Deepmind control suite. *CoRR*, abs/1801.00690, 2018. URL <http://arxiv.org/abs/1801.00690>.

Emanuel Todorov, Tom Erez, and Yuval Tassa. Mujoco: A physics engine for model-based control. In *IEEE/RSJ International Conference on Intelligent Robots and Systems (IROS)*, pages 5026–5033, 2012. doi: 10.1109/IROS.2012.6386109.

Filippo Vannella, Grigoris Iakovidis, Ezeddin Al Hakim, Erik Aumayr, and Saman Feghhi. Remote electrical tilt optimization via safe reinforcement learning. In *IEEE Wireless Communications and Networking Conference*, pages 1–7. IEEE, 2021. doi: 10.1109/WCNC49053.2021.9417363.

## Appendix A.

This appendix contains the proof of lemma 1.

**Proof** [Proof of Lemma 1] For the sake of notation, let  $V_0 = V_{M_0}^\pi$  and  $V_1 = V_{M_1}^\pi$ . Further, define  $\Delta V(s) = V_0(s) - V_1(s)$ ,  $\Delta P(s'|s, a) = P_0(s'|s, a) - P_1(s'|s, a)$ .

$$\begin{aligned}\Delta V(s) &= \mathbb{E}_{a \sim \pi(s)} \left[ \gamma \mathbb{E}_{s'_0 \sim P_0(s, a)} [V_0(s'_0)] - \gamma \mathbb{E}_{s'_1 \sim P_1(s, a)} [V_1(s'_1)] \right], \\ &= \gamma \mathbb{E}_{a \sim \pi(s)} \left[ \mathbb{E}_{s'_0 \sim P_0(s, a)} [V_0(s'_0)] - \gamma \mathbb{E}_{s'_1 \sim P_1(s, a)} [V_1(s'_1) \pm V_0(s'_1)] \right], \\ &= \gamma \mathbb{E}_{a \sim \pi(s)} \left[ \underbrace{\left( \mathbb{E}_{s'_0 \sim P_0(s, a)} [V_0(s'_0)] - \mathbb{E}_{s'_1 \sim P_1(s, a)} [V_0(s'_1)] \right)}_{(a)} + \gamma \underbrace{\mathbb{E}_{s'_1 \sim P_1(s, a)} [\Delta V(s'_1)]}_{(b)} \right].\end{aligned}$$

By expanding (b) recursively, we find that

$$\Delta V(s) = \frac{\gamma}{1 - \gamma} \mathbb{E}_{z \sim \mu_1^\pi(s), a \sim \pi(z)} \left[ \underbrace{\left( \mathbb{E}_{s'_0 \sim P_0(z, a)} [V_0(s'_0)] - \mathbb{E}_{s'_1 \sim P_1(z, a)} [V_0(s'_1)] \right)}_{(a)} \right]$$

where  $\mu_1^\pi(s)$  is the discounted policy distribution induced by  $\pi$  starting in  $s$  in model  $M_1$ . By Pinsker's inequality we bound (a) as follows:

$$\left| \mathbb{E}_{s'_0 \sim P_0(s, a)} [V_0^\pi(s'_0)] - \mathbb{E}_{s'_1 \sim P_1(s, a)} [V_0^\pi(s'_1)] \right| \leq \|P_0(s, a) - P_1(s, a)\|_1 \|V_0\|_\infty.$$

Consequently, we have  $|\Delta V(s)| \leq \sqrt{2} \frac{\gamma}{1 - \gamma} \|V_0\|_\infty \mathbb{E}_{z \sim \mu_1^\pi(s), a \sim \pi(z)} \left[ \sqrt{\text{KL}(P_0(z, a), P_1(z, a))} \right]$ . ■

## Appendix B.

This appendix contains the hyperparameters of the algorithms for all the experiments.

### B.1. Antenna environment

Parameter	Value
Actor hidden layers	[64, 64, 64]
Critic hidden layers	[64, 64, 64]
Actor lr	$3 \cdot 10^{-4}$
Critic lr	$3 \cdot 10^{-4}$
Buffer size	10000
Policy distribution	Tanh squashed Gaussian
Exploration type	Sample from policy
Random time steps	0
Learning starts time step	100
$\gamma$	0.9
$\tau$	$5 \cdot 10^{-3}$
Target network update	Every other time step
Batch size	128
Dueling Q	No
Entropy lr	$3 \cdot 10^{-4}$
$\alpha_0$	1
Target entropy	-1
Metric smoothing	5 episodes
Time steps per epoch	500
Number of epochs	20

Table 2: Hyperparameters for SAC in the antenna environment.

Parameter	Value
Transition model hidden layers	[64, 64, 64]
Model lr	$10^{-3}$
Rollout length	10
Model batch size	128
Model rollouts	1280

Table 3: Additional hyperparameters used for the model-based component in the antenna environment.

Parameter	Value
Actor hidden layers	[64, 64, 64]
Critic hidden layers	[64, 64, 64]
Actor lr	$3 \cdot 10^{-4}$
Critic lr	$3 \cdot 10^{-4}$
Buffer size	10000
Policy distribution	Deterministic
Exploration type	Epsilon-greedy
Exploration $\epsilon_0$	1
Exploration $\epsilon_{final}$	0.01
Exploration decay time steps	3000
Random time steps	0
Learning starts time step	100
$\gamma$	0.9
$\tau$	$5 \cdot 10^{-3}$
Batch size	128
Dueling Q	No
Metric smoothing	5 episodes
Time steps per epoch	500
Number of epochs	20

Table 4: Hyperparameters used for DQN in the antenna environment.

## B.2. MuJoCo environments

The parameters used by MBPO, SAC and MBRPL for Hopper, Walker and Truncated Ant can be seen below. The corrected policy  $\pi_\phi^b$  was created by adding the mean of the baseline policy's output

Parameter	Value
Training steps	125000
Epoch length	1000
Initial exploration steps	5000
Model lr	$10^{-3}$
Model L2	$10^{-5}$
Model batch size	256
Model validation ratio	0.2
Model hidden layers	[200, 200, 200, 200]
Ensemble size	7
Freq. train model	250
Model rollouts per steps	400
Rollout schedule	[20, 150, 1, 15]
SAC updates per step	20
SAC $\gamma$	0.99
SAC $\tau$	$5 \cdot 10^{-3}$
SAC $\alpha_0$	1
SAC policy	Gaussian
SAC target update interval	1
SAC auto entropy tuning	True
SAC hidden layers	[256, 256]
SAC lr	$3 \cdot 10^{-4}$
SAC batch size	256

Table 5: Hyperparameters on Hopper.

Parameter	Value	Parameter	Value
Training steps	$3 \cdot 10^5$	Training steps	$3 \cdot 10^5$
Epoch length	1000	Epoch length	1000
Initial exploration steps	5000	Initial exploration steps	5000
Model lr	$10^{-3}$	Model lr	$3 \cdot 10^{-4}$
Model L2	$10^{-5}$	Model L2	$5 \cdot 10^{-5}$
Model batch size	256	Model batch size	256
Model validation ratio	0.2	Model validation ratio	0.2
Model hidden layers	[200, 200, 200, 200]	Model hidden layers	[200, 200, 200, 200]
Ensemble size	7	Ensemble size	7
Freq. train model	250	Freq. train model	250
Model rollouts per steps	400	Model rollouts per steps	400
Rollout schedule	[20, 150, 1, 1]	Rollout schedule	[20, 100, 1, 25]
SAC updates per step	20	SAC updates per step	20
SAC $\gamma$	0.99	SAC $\gamma$	0.99
SAC $\tau$	$5 \cdot 10^{-3}$	SAC $\tau$	$5 \cdot 10^{-3}$
SAC $\alpha_0$	0.2	SAC $\alpha_0$	0.2
SAC policy	Gaussian	SAC policy	Gaussian
SAC target update interval	4	SAC target update interval	4
SAC auto entropy tuning	False	SAC auto entropy tuning	False
SAC hidden layers	[1024, 1024]	SAC hidden layers	[1024, 1024]
SAC lr	$10^{-4}$	SAC lr	$10^{-4}$
SAC batch size	256	SAC batch size	256

Table 6: Hyperparameters on Walker2d-v3

Table 7: Hyperparameters on truncated ant.

## Appendix C.

This section provides details on the model and policy training steps that we used for MBRPL in the antenna tilt problem. During training, these two steps were performed for each step in the real environment. See Algorithm 1 for more details.

### C.1. Model learning step

We trained a single model using a mean squared error supervised loss. Firstly, under the Markov assumption:

$$p(s_{0:T} \mid a_{0:T-1}) = \rho(s_0) \prod_{t=1}^{T-1} p(s_{t+1} \mid s_t, a_t). \quad (2)$$

Furthermore, we assume that  $p_\theta(s_{t+1} \mid s_t, a_t)$  is normally distributed:

$$p_\theta(\cdot \mid s_t, a_t) = \mathcal{N}(\mu_\theta(s_t, a_t), \Sigma_\theta(s_t, a_t)), \quad (3)$$

and we use a dense neural network parameterized by  $\theta$  to output the mean  $\mu_\theta$  and the diagonal co-variance  $\Sigma_\theta$ . The loss is calculated using a MSE between a batch of the normalized *true* states  $\hat{s}$

and the mean of 10 batches of the normalized *generated* states  $\bar{\mathbf{s}}_{gen}^{(b)}$ :

$$L_\theta = \frac{1}{B \cdot d} \sum_{b=0}^{B-1} \|\hat{\mathbf{s}}^{(b)} - \bar{\mathbf{s}}_{gen}^{(b)}\|_2^2 \quad (4)$$

Here,  $\hat{\mathbf{s}}^{(b)}$  indicates the  $b$ -th state vector in the batch, and similarly for  $\bar{\mathbf{s}}_{gen}^{(b)}$ . The states are re-scaled by element-wise division with  $\mathbf{s}_{max} - \mathbf{s}_{min}$ , which is the difference between the upper and lower bounds of the state-space. Also note that  $d$  is the dimension of the state-space and  $B$  the batch size. The parameter  $\theta$  is then learned via gradient descent using the re-sampling trick on the generated data. One model learning step is performed on one batch of data for each step in the true environment.

## C.2. Policy learning step

The residual policy is trained using generated data from the learned transition model  $p_\theta(s' | s, a)$ .  $H$  actor-critic updates are made per sample batch from the buffer of real experiences. We used the actor-critic loss functions of the SAC method [Haarnoja et al. \(2018b\)](#). Pseudocode for a single policy update step can be seen in Algorithm 2. One such learning step is performed on a batch of data sampled from the buffer for each step in the real environment.

---

### Algorithm 2 Policy learning step

---

**Input:** Batches  $(\mathbf{s}_t, \mathbf{a}_t, \mathbf{r}_t, \mathbf{s}_{t+1})$ , transition model  $p_\theta$ , baseline policy  $\pi_b$ , residual policy  $\pi_\phi^b$ , critic  $Q_\psi$ , reward function  $r$

- 1: **for**  $\tau$  from  $t$  to  $t + H$  **do**
- 2:   **if**  $\tau > t$  **then**
- 3:     Sample action batch  $\mathbf{a}_\tau$  using  $\pi_\phi^b(\mathbf{s}_\tau)$
- 4:      $\mathbf{s}_{\tau+1} \sim p_\theta(\mathbf{s}' | \mathbf{s}_\tau, \mathbf{a}_\tau)$  {Predict next state batch}
- 5:      $\mathbf{r}_\tau = r(\mathbf{s}_\tau, \mathbf{a}_\tau, \mathbf{s}_{\tau+1})$
- 6:   **end if**
- 7:   Perform actor-critic learning step on batches  $(\mathbf{s}_\tau, \mathbf{a}_\tau, \mathbf{r}_\tau, \mathbf{s}_{\tau+1})$
- 8: **end for**

---

## Appendix D.

This appendix contains more detail about the mathematical models used to compute the coverage, capacity and quality KPIs used in the antenna tilt environment. The mathematical models for computing the signal strength, quality and interference is consistent with previous work [Bouton et al. \(2021\)](#); [Farooq et al. \(2019\)](#).

There is a trade-off between coverage, capacity and quality when controlling the antenna tilt [Buenestado et al. \(2017\)](#); [Vannella et al. \(2021\)](#). This is illustrated in Fig. 4, for the simplified case of two antennas. Increasing the tilt (down tilting) concentrates the antenna signal to a smaller area, which can lead to coverage holes, shown in the top illustration. However, a more concentrated signal can lead to a higher capacity and quality for the users inside the covered area. On the other hand, a small down-tilt angle will lead to a large area being covered, but the signal will be relatively weak, resulting in lower capacity. A too small down-tilt angle can also lead to interference with neighboring antennas, like in the second illustration. The optimal setting is found somewhere in the middle, as in

the third illustration.

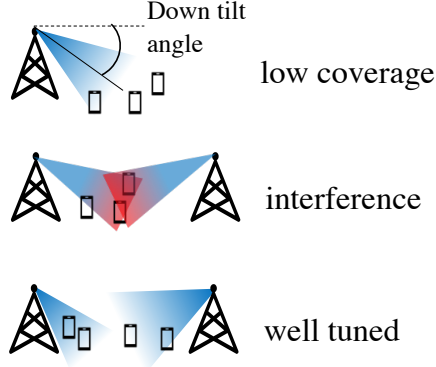


Figure 4: The effect of changing the antenna tilt-angle. A large down-tilt angle like in figure a) leads to bad coverage but potentially high capacity and quality. A too small down-tilt angle can lead to good coverage, but also lower capacity and quality (figure b). The optimal angle is found somewhere in between, shown in figure c).

A common way to measure coverage is via the Reference Signal Received Power (RSRP), which is the power of the signal received by a user attached to a cell Dreifuerst et al. (2021); Farooq et al. (2019). We denote the RSRP of user  $u$  attached to cell  $c$  as  $\rho_c^u$ . The RSRP is a function of the transmitted power from the antenna  $P_c$ , the gain of the antenna  $G_c^u$ , and path loss  $L_c^u$ :  $\rho_c^u = P_c G_c^u L_c^u$ . The gain is a function of the down-tilt angle  $w$ , and the path-loss depends on obstacles (such as buildings and trees) and the medium of transmission. Since RSRP is a function of  $w$  and the users decide which cell to attach to based on the RSRP, the down-tilt angle affects how many users are attached to a cell. There are a number of ways to use RSRP to measure the coverage of the entire cell. We used the average log RSRP across users attached to that cell:  $COV_c = \frac{1}{|U_c|} \sum_{u \in U_c} \log \rho_c^u$ , where  $U_c$  is the set of indices of users in cell  $c$ . We decided to use the logarithmic value in order to down-scale the otherwise large values, which helps for training the deep learning models (environment model, policy or value function).

The quality can be measured via the Signal to Interference and Noise Ratio (SINR). The SINR  $\gamma$  of user  $u$  attached to cell  $c$  can be defined as the corresponding RSRP value, divided by a noise term plus the RSRP from all other cells:

$$\gamma_c^u = \frac{\rho_c^u}{\kappa + \sum_{i \in C \setminus c} \rho_i^u}. \quad (5)$$

Here,  $\kappa$  is the noise term and  $C$  the set of cell indices. We measured the quality in a cell as the average log SINR over users:  $QUAL_c = \frac{1}{|U_c|} \sum_{u \in U_c} \log \gamma_c^u$ .

The throughput for user  $u$  attached to cell  $c$  can be defined as:

$$T_c^u = \frac{\omega_B n_B}{|U_c|} \log_2(1 + \gamma_c^u). \quad (6)$$

Here,  $\omega_B$  is the bandwidth per physical resource block, and it is assumed that each user is assigned the same number of physical resource blocks  $n_B$ . We measure the capacity for a cell with the average log throughput across users:  $CAP_c = \frac{1}{|U_c|} \sum_{u \in U_c} \log T_c^u$ .

All three metrics were normalized to have mean  $\mu \approx 0$  and standard deviation  $\sigma \approx 1$ . In practice, we had to limit the standard deviation further for some of the metrics to prevent outlier data.

We defined the action space as  $\mathcal{A} = \{\Delta w_c \mid \Delta w_c \in [-1^\circ, 1^\circ]\}$ . The state-space was defined as  $\mathcal{S} = \{(w_c, COV_c, CAP_c, QUAL_c)_{c=1}^C \mid w_c \in [0^\circ, 15^\circ]\}$ . We defined the reward function as  $r(s_t, a_t, s_{t+1}) = COV_{c,t+1} + CAP_{c,t+1} + QUAL_{c,t+1}$ . The true transition probabilities  $p(s' \mid s, a)$  were unknown and modeled by a proprietary network simulator [Asplund et al. \(2018\)](#).